CLEAN
Soil Air Water

Tahir Ali Akbar [1]
Quazi K. Hassan [2]
Gopal Achari [1]

[1]Department of Civil Engineering, Schulich School of Engineering, University of Calgary, Calgary, Alberta, Canada
[2]Department of Geomatics Engineering, Schulich School of Engineering, University of Calgary, Calgary, Alberta, Canada

Research Article

Development of Remote Sensing Based Models for Surface Water Quality

The objectives of this paper were to develop, evaluate, and apply the remote sensing based models for Canadian Water Quality Index (CWQI) and turbidity for the Bow River of Alberta. We used 31 scenes of Landsat-5 TM satellite data to establish the relationship between the planetary reflectance and the monthly ground measured data for the period of 5 years (i.e. 2006–2010). The four spectral bands (i.e. blue, green, red, and near infrared) were used to obtain the most suitable models from 26 different band combinations. The co-efficients of determination on the basis of red band were 0.91 for the CWQI model and 0.82 for the turbidity model. The best-fit models were validated with ground measured data and found that: 72% of the data showed 100% matching for the CWQI model and 83% of the data for the turbidity model. The Landsat-5 TM based CWQI and turbidity models were applied on all the scenes to obtain five CWQI classes (i.e. excellent, good, fair, marginal and poor), and six classes of turbidity (i.e. 0–10 NTU, 10–20 NTU, 20–30 NTU, 30–40 NTU, 40–50 NTU, >50 NTU). On the basis of percentages obtained for CWQI and turbidity classes, the ranks of years in terms of water quality from best to worst were: 2009, 2006, 2008, 2010, and 2007 respectively. The variation of river water quality in different years of interest was associated with the climatic changes. The most deteriorated water quality noted in two natural sub-regions included mixed grass and dry mixed grass, which could be related to irrigation-based farming.

Keywords: Bow River; Canadian Water Quality Index; Landsat-5 TM; Turbidity

Received: January 1, 2013; *revised:* August 13, 2013; *accepted:* August 18, 2013

DOI: 10.1002/clen.201300001

1 Introduction

Water extends approximately 71% of earth's surface and it is also imperative for the existence and sustainability of living organism on the earth surface [1]. The freshwater is just 2.5% of the earth's water. About 0.3% of freshwater is found in rivers, lakes, and atmosphere [2]. In general, the understanding of the water quality plays a critical role prior to utilize for various purposes including drinking [3]. In this paper, we opted to understand the surface water quality for the Bow River, which is a major river in the Canadian province of Alberta having a total length of 587 km, and a main source of drinking water for many communities of the province [4].

The surface water quality of the Bow River is measured every month at three fixed sampling sites (i.e. Carseland, Cluny, and Ronalane) for different water quality variables using the traditional methods. In general, these methods provide accurate measurement. However, these may not be feasible means to sample the entire river due to the huge involvement of labor and cost. Currently, the measured data of water quality variables at the sampling sites of the Bow River are grouped into five classes (i.e. excellent, good, fair, marginal and poor) using the framework of Canadian Water Quality Index (CWQI: see details in Section 2.5) [5]. These classes are obtained on the basis of fixed-point locations, which do not represent the spatial dynamics of the entire river.

In another study, we classified the surface water quality of major rivers of Alberta on the basis of clusters. We observed higher (deteriorated water quality) clusters (i.e. 4 and 5) for the rivers during the growing season (April 1–September 30) as compared to lower clusters (i.e. 1, 2, and 3) in winter months (Oct 1–March 31). During the growing season, the snowmelt wash various materials from the land surface into the rivers due to anthropogenic activities related to different types of land use/cover. Turbidity was found to be a dominant parameter associated with the deterioration in water quality during the growing season [6]. On this basis, we considered turbidity separately besides CWQI in this study. For the Bow River, the turbidity is measured at fixed sampling location, which does not represent the mean turbidity for the whole water body [7].

In order to address the spatial variability in water quality real time data, remote sensing-based methods were found to be alternative and efficient ones [8–10]. The remote sensing methods are suitable to analyze: (i) spatial variability over a large geographic area, (ii) temporal trends over certain periods of interests, and (iii) the conditions of the water bodies in remote areas. In remote sensing, optical remote sensors are used for monitoring the water quality-related variables. The most commonly used sensors include the use of Landsat-7 ETM [11, 12], Landsat-5 TM [13, 14], MODIS [15], NOAA AVHRR [16], and SPOT HVR [17] among others. In most of the

Correspondence: Dr. Quazi K. Hassan, Department of Geomatics Engineering, Schulich School of Engineering, University of Calgary, Calgary, Alberta, Canada
E-mail: qhassan@ucalgary.ca

Abbreviations: BOR-1 BOR-2 BOR-3, sampling sites of Bow River; **B**, blue; **CWQI**, Canadian Water Quality Index; **G**, green; **NDVI**, normalized difference vegetation index; **NIR**, near infrared; **NTU**, nephelometric turbidity unit; **R**, red

The copyright has been changed after first publication.

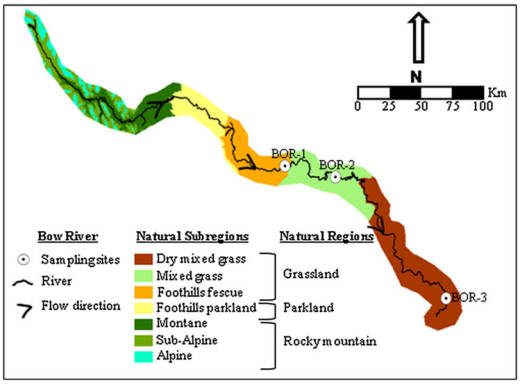

Figure 1. Natural sub-regions for the Bow River of Alberta.

instances, the spectral bands used in these studies included blue (B), green (G), red (R), and near infrared (NIR) [11–17]. The observed planetary reflectance from these bands was used to study water quality variables including suspended sediment, turbidity, Secchi disk depth, and chlorophyll-a [12, 13, 18, 19].

In another study, we classified and analyzed the surface water quality for twelve major rivers of Alberta. We developed a surface water quality classification system using principal component analysis, total exceedance model and clustering technique. From principal component analysis, we identified seven major principal components, which were the indicators of watershed geology, mineralization, and anthropogenic activities related to land use/cover. The principal components were used to identify the dominant parameters. The normalized data of dominant parameters were used to develop a total exceedance model. The exceedance values were used to determine the patterns for the development of five clusters. The water quality deteriorates as the cluster number increased from cluster 1 to cluster 5. The clusters showed reasonably strong agreements (i.e. 80–90%) against the classes of CWQI. The dominant clusters during the growing and winter seasons were used for the spatial and temporal patterns of the surface water quality of rivers [6].

In the present study, we have tested remote sensing-based methods for acquiring CWQI and turbidity classes for assessing both spatial and temporal dynamics of the Bow River. The specific objectives of this paper are to: (i) develop and evaluate remote sensing based models to acquire CWQI classes using the planetary reflectance of Landsat-5 TM and ground measured data, (ii) develop and evaluate remote sensing based models to retrieve turbidity using the planetary reflectance of Landsat-5 TM and in situ data, (iii) apply the selected models to classify the source waters of the Bow River into CWQI and turbidity classes for spatial and temporal analysis, and (iv) study the impact of natural sub-regions on Bow River water quality.

2 Materials and methods

2.1 Study area

The Bow River originates from Bow Glacier located on the north of Lake Louise in Alberta. It flows in southeastern direction and merges with Oldman River to make South Saskatchewan River. The Bow River is surrounded by three natural regions including Grassland, Parkland, and Rocky Mountain. These regions are classified into six natural sub-regions (i.e. dry mixed grass, mixed grass, foothills fescue, foothills parkland, montane, and sub-alpine) as shown in Fig. 1. For these sub-regions, the range for: (i) the estimated length of the Bow River flowing through each natural sub-region is from 39 to 171 km, (ii) the mean annual temperature is from −0.1 to 4.4°C, and (iii) the mean annual precipitation is from 333 to 755 mm as given in Tab. 1. The main vegetation type for each of the sub-regions is also mentioned in Tab. 1. The drainage area for the Bow River is 25 000 km^2 [4]. The major municipality along the river is the City of Calgary (i.e. having a population of 1 096 833 according to 2011 census), which receives drinking water from this river [20]. The mean annual flow of the river near Calgary is 91.1 m^3/s [21]. The water flow is controlled by two dams (Bearspaw Dam and Ghost Dam) constructed on the Bow River for the supply of electricity to the City of Calgary [22]. The surface water of Bow River allocated for various purposes include: (i) 71% for irrigation, (ii) 18% for municipal, (iii) 4% for water management, (iv) 2% for management of wildlife, (v) 2% for dewatering, and (vi) 2% for commercial [23].

2.2 Satellite and water quality data

We used 31 scenes of Landsat-5 TM multispectral image data for the different dates during the period 2006–2010 as listed in Tab. 2. The size of each scene was 185 km × 172 km. The spectral bands which were used in this study were (i) blue, (ii) green, (iii) red, and (iv) NIR. The spatial resolution for each of these spectral bands was 30 m. The raw satellite data was downloaded from the United States Geological Survey Global Visualization Viewer in GeoTIFF format with the Level 1T correction [24]. The Level 1T is the standard terrain correction in which systematic radiometric and geometric accuracy is provided using the ground control points and the topographic accuracy is obtained by using the digital elevation model [25]. The scenes of Landsat-5 TM were selected on the basis of the least cloud cover, least snow, and closeness to the sampling days. In total, we used ground measured data for 37 days at three sampling locations of the Bow River in 2006–2010 to develop and validate models using the planetary reflectance of 31 scenes of Landsat-5 TM. The sampling locations and the dates for the ground water quality data and Landsat-5 TM scenes are given in Tab. 2.

Table 1. Characteristics of natural sub-regions for Bow River

Natural sub-region	Bow River length (km)	Mean annual temperature (°C)	Mean annual precipitation (mm)	Main vegetation
Dry mixed grass	171	4.2	333	Grasslands and shrublands
Mixed grass	107	4.4	394	Agriculture and native grassland
Foothills fescue	87	3.9	470	Mountain perennial and wheat grasses
Foothills parkland	63	3.0	517	Aspen forests and grasslands
Montane	120	2.3	589	Aspen, pine, fir and spruce forests and grasslands
Sub-alpine	39	−0.1	755	Mixed conifer forests

Table 2. Data used for development and evaluation of models for CWQI and turbidity during 2006–2010

River water sampling			Landsat-5 TM scene			
No.	Site	Date	No.	Acquisition date	Path	Row
1	Carseland	26-Apr-06	1	24-Apr-06	41	25
2	Cluny	25-Apr-06				
3	Carseland	23-May-06	2	17-May-06	42	24
4	Carseland	12-Jul-06	3	13-Jul-06	41	25
5	Cluny	12-Jul-06				
6	Ronalane	25-Jul-06	4	22-Jul-06	40	25
7	Carseland	31-Aug-06	5	30-Aug-06	41	25
8	Cluny	31-Aug-06				
9	Ronalane	19-Sep-06	6	24-Sep-06	40	25
10	Carseland	23-Nov-06	7	18-Nov-06	41	25
11	Cluny	23-Nov-06				
12	Carseland	19-Jun-07	8	21-Jun-07	42	24
13	Ronalane	25-Jun-07	9	23-Jun-07	40	25
14	Cluny	26-Jun-07	10	30-Jun-07	41	25
15	Carseland	23-Jul-07	11	23-Jul-07	42	24
16	Carseland	28-Apr-08	12	29-Apr-08	41	25
17	Carseland	14-May-08	13	15-May-08	41	25
18	Cluny	14-May-08				
19	Carseland	17-Jun-08	14	23-Jun-08	42	24
20	Ronalane	16-Jul-08	15	11-Jul-08	40	25
21	Carseland	15-Jul-08	16	18-Jul-08	41	25
22	Ronalane	21-Aug-08	17	28-Aug-08	40	25
23	Ronalane	14-Oct-08	18	15-Oct-08	40	25
24	Carseland	26-May-09	19	25-May-09	42	24
25	Ronalane	25-May-09	20	27-May-09	40	25
26	Carseland	15-Jun-09	21	10-Jun-09	42	24
27	Carseland	20-Jul-09	22	21-Jul-09	41	25
28	Carseland	17-Aug-09	23	22-Aug-09	41	25
29	Cluny	17-Aug-09				
30	Cluny	15-Sep-09	24	7-Sep-09	41	25
31	Carseland	14-Sep-09	25	14-Sep-09	42	24
32	Carseland	19-Oct-09	26	25-Oct-09	41	25
33	Cluny	21-Apr-10	27	19-Apr-10	41	25
34	Carseland	19-Apr-10	28	26-Apr-10	42	24
35	Carseland	10-May-10	29	12-May-10	42	24
36	Carseland	15-Jul-10	30	15-Jul-10	42	24
37	Ronalane	18-Aug-10	31	18-Aug-10	40	25

The water quality data were obtained from Alberta Environment and listed in Tab. 3 with Alberta River Water Quality Index objectives [26–29].

2.3 Image processing

The satellite scenes were processed to make them workable for the purpose of this research. The operations applied for processing are briefly explained in the following sub-sections:

2.3.1 Conversion of digital numbers into spectral radiance

In the first step, we converted the raw digital numbers of all the Landsat-5 TM images into spectral radiance using Eq. (1) [25] as follows:

$$L_\lambda = \left[\left(\frac{L_{\max\lambda} - L_{\min\lambda}}{\mathrm{DN}_{\max} - \mathrm{DN}_{\min}}\right) \times (\mathrm{DN} - \mathrm{DN}_{\min})\right] + L_{\min\lambda} \quad (1)$$

where L_λ = spectral radiance at the sensor's aperture ($\mathrm{W\,m^{-2}\,sr^{-1}\,\mu m^{-1}}$), DN = quantized calibrated pixel value, $L_{\min\lambda}$ = spectral radiance that is scaled to QCALMIN ($\mathrm{W\,m^{-2}\,sr^{-1}\,\mu m^{-1}}$), $L_{\max\lambda}$ = spectral radiance that is scaled to QCALMAX ($\mathrm{W\,m^{-2}\,sr^{-1}\,\mu m^{-1}}$), $\mathrm{DN}_{\min}$ = minimum quantized calibrated pixel value (corresponding to $L_{\min\lambda}$) in DN, and $\mathrm{DN}_{\max}$ = maximum quantized calibrated pixel value (corresponding to $L_{\max\lambda}$) in DN.

The values of $L_{\min\lambda}$, $L_{\max\lambda}$, $\mathrm{DN}_{\min}$ and $\mathrm{DN}_{\max}$ in Eq. (1) were obtained from the metadata files.

Table 3. Alberta River Water Quality Index objectives for 17 variables [26–29]

Variable	Objective	Variable	Objective	Variable	Objective
Water temperature	15°C	Total phosphorus	0.05 mg/L	Sodium	200 mg/L
Dissolved oxygen	6.5 mg/L	Total nitrogen	1 mg/L	Fluoride	1.5 mg/L
Turbidity	5 NTU	pH	6.5 and 8.5	Fecal coliform	100 CPU/100 mL
True color	15 Pt Co units	Total hardness	500 mg/L	Manganese	0.05 mg/L
Dissolved organic carbon	5 mg/L	Chloride	250 mg/L	Iron	0.3 mg/L
Total dissolved solids	500 mg/L	SO_4	500 mg/L		

2.3.2 Conversion from spectral radiance to planetary reflectance

In the second step, the spectral radiance was converted into planetary reflectance using Eq. (2) [25] as follows:

$$\rho_\rho = \left[\frac{\pi L_\lambda d^2}{\mathrm{ESUN}_\lambda \cos\theta_s}\right] \quad (2)$$

where ρ_ρ = unitless planetary reflectance, $\pi = 3.141592654$, L_λ = spectral radiance at the sensor's aperture, d = earth–sun distance in astronomical units, ESUN_λ = mean solar exo-atmospheric irradiance, and θ_s = solar zenith angle (°).

The value of: (i) d was obtained from Science Data Users Handbook [30], (ii) ESUN_λ for all bands of TM sensors were obtained from Chander and Markham [31], (iii) θ_s was obtained from the formula (i.e. $\theta_s = 90° -$ sun elevation angle), where the sun elevation angle was obtained from the metadata file of each satellite images.

2.3.3 Normalized Difference Vegetation Index (NDVI)

Finally, we calculated normalized difference vegetation index (NDVI: a measure of vegetation greenness) using Eq. (3) [32] as follows:

$$\mathrm{NDVI} = \frac{\rho_{\mathrm{NIR}} - \rho_{\mathrm{R}}}{\rho_{\mathrm{NIR}} + \rho_{\mathrm{R}}} \quad (3)$$

where ρ_{NIR} = reflectance of NIR band, and ρ_{R} = reflectance of red band.

Such NDVI calculations were performed over the Bow River sampling sites (BOR-1, BOR-2, BOR-3) in all scenes of 37 data records in order to determine the possible contamination of sampling site pixels from other landuses (e.g. roads, agriculture, vegetation, and barren land, etc.). The negative NDVI values (i.e. between 0 and −1) indicated the presence of water in the pixels whereas positive NDVI values showed the possible contamination due to other landuses [33]. In case of a positive NDVI value for any sampling site pixel, we considered the reflectance value of a nearest neighboring water pixel.

2.4 CWQI

Using Eq. (4), we calculated CWQI for all three sampling sites of Bow River during the period 2006–2010 using the measured data of seventeen variables on the basis of Alberta River Water Quality Index objectives as given in Tab. 3 [5]:

$$\mathrm{CWQI} = 100 - \left(\frac{\sqrt{F_1^2 + F_2^2 + F_3^2}}{1.732}\right) \quad (4)$$

where F_1, F_2, F_3 are scope, frequency, and amplitude, respectively. The equations to calculate these three factors are given in Tab. 4. The quantitative values (i.e. 0–100) obtained from Eq. (4) were divided into five classes: (i) 95–100 = 1 (excellent), (ii) 80–94 = 2 (good), (iii) 60–79 = 3 (fair), (iv) 45–59 = 4 (marginal), and (v) 0–44 = 5 (poor) [5]. The CWQI classes were produced for 37 data records as given in Tab. 2.

2.5 Models for CWQI and turbidity from planetary reflectance of Landsat-5 TM data

On the basis of literature review for the relationship of bands with the variables of water quality, we developed 26 individual empirical models in determining both CWQI and turbidity as a function of the spectral bands of B, G, R and NIR [10–18]. The specific inputs of these models were: B, G, R, NIR, G/B, B/R, R/B, NIR/B, R/G, NIR/G, B + G, B + R, B + NIR, G + R, G + NIR, R + NIR, B + G + R, B + G + NIR, G + R + NIR, B + G + R + NIR, (B/NIR) + G, (B/NIR) + B, (B/R) + R, (B/R) + G, (B/R) + B, and (NIR/B) + NIR. We used regression analysis technique to obtain the quantitative relationship beween the satellite based planetary reflectances and water quality variables to develop the empirical models [8–18]. We used 23 data records (i.e. Landsat-5 TM as well as the ground data) for the development of models to obtain CWQI classes and turbidity from the planetary reflectance. The remaining 14 data records were used to validate the selected best models. In all these models, CWQI and turbidity were the dependent variables whereas the bands were the independent variables. CWQI and turbidity were plotted on the vertical axis and bands on the horizontal axis. Each model represents: (i) a unique band formula, (ii) an intercept, and (iii) a slope. The intercept of dependable variables is the distance from the origin to the point where the line crosses the vertical axis. Slope is the amount of change for dependent variables corresponding to one-unit increase in band formula. The intercept and slope were calculated using the least square regression method to obtain a line of best fit. The strength of correlations between the planetary reflectance and in situ turbidity and CWQI for the development and validation of the models were obtained based on co-efficient of determination (r^2) [34]. On the basis of r^2 values, we identified the significant empirical models for CWQI and turbidity.

2.6 Spatial and temporal analysis for the Bow River

We subset all the scenes of interest to extract the Bow River. The NDVI was calculated for the Bow River to extract the pixels with water and remove the pixels contaminated with other land use types. We selected the most suitable empirical models for CWQI and turbidity on the basis of r^2 values. The selected CWQI model was applied on 31 scenes of Landsat-5 TM to obtain the spatial distribution for five classes (i.e. as described in Section 2.4) along the Bow River. Similarly, the selected turbidity model was applied on these scenes to obtain the spatial distribution of turbidity. The turbidity values were divided into

Table 4. Equations used for calculation of CWQI and identifying classes using the data

$$F_1(\mathrm{Scope}) = \left(\frac{\text{Number of failed variables}}{\text{Total number of variables}}\right) \times 100$$

$$F_2(\mathrm{Frequency}) = \left(\frac{\text{Number of failed tests}}{\text{Total number of tests}}\right) \times 100$$

$$\text{Excursion } i = \left(\frac{\text{Objective } j}{\text{Failed test value } i}\right) - 1$$

$$\text{Excursion } i = \left(\frac{\text{Failed test value } i}{\text{Objective } j}\right) - 1$$

$$\mathrm{NSE} = \left(\frac{\sum_{i=1}^{n} \text{excursion } i}{\text{Number of tests}}\right)$$

$$F_3(\mathrm{amplitude}) = \left(\frac{\mathrm{NSE}}{0.01\,\mathrm{NSE} + 0.01}\right)$$

Table 5. Models developed for mapping spatial distribution of CWQI classes for the Bow River using the first four spectral bands (i.e. blue, green, red, and NIR) of Landsat-5 TM satellite data

Model no.	Model	r^2	Model no.	Model	r^2
1	28.072 R + 0.5785	0.91	14	15.044 (B + NIR) + 0.2322	0.54
2	14.816 (G + R) + 0.1715	0.84	15	−0.861 (B/R) + 3.6939	0.36
3	16.031 (R + NIR) + 0.6253	0.82	16	−0.8493 [(B/R) + G] + 3.7451	0.33
4	10.789 (G + R + NIR) + 0.2845	0.81	17	−0.8478 [(B/R) + R] + 3.7247	0.32
5	5.3855 (R/G) − 1.6506	0.77	18	−0.8108 [(B/R) + B] + 3.6895	0.32
6	8.2823 (B + G + R + NIR) − 0.0287	0.76	19	17.588 B + 0.6427	0.30
7	10.241 (B + G + R) − 0.1374	0.75	20	0.982 (R/B) + 1.648	0.17
8	14.834 (B + R) − 0.0091	0.73	21	−0.2439 [(B/NIR) + G] 2.8986	0.12
9	16.705 (G + NIR) + 0.2038	0.72	22	−0.2427 [(B/NIR) + B] + 2.8986	0.12
10	29.187 G − 0.103	0.71	23	1.0725 [(NIR/B) + NIR] + 1.7535	0.11
11	10.852 (B + G + NIR) − 0.0855	0.65	24	1.7162 (NIR/G) + 1.4118	0.10
12	30.554 NIR + 0.9825	0.58	25	0.9607 (NIR/B) + 1.8524	0.08
13	13.808 (B + G) − 0.1391	0.57	26	0.2513 (G/B) + 2.0777	0.01

six classes which are: (i) 0–10 nephelometric turbidity units (NTU), (ii) 10–20 NTU, (ii) 20–30 NTU, (iv) 30–40 NTU, (v) 40–50 NTU and (vi) >50 NTU [35]. CWQI classes could vary from 1 to 5 with the increase in the concentrations of variables. For example lower turbidity classes might indicate lower cluster numbers whereas higher turbidity classes could represent higher cluster numbers. For both turbidity and CWQI, the percentage accumulated by each class was obtained by dividing the pixels of each class by the total pixels of all classes during each year of interest during 2006–2010. Finally, we overlaid maps for CWQI classes for the selected period on the natural sub-regions (i.e. Fig. 1).

3 Results and discussion

3.1 Empirical models for determining CWQI classes

We developed 26 empirical models for determining CWQI classes as given in Tab. 5. These empirical models could be used to obtain the spatial distribution of CWQI classes using the planetary reflectance of bands for any periods. The slopes in CWQI were the constant numbers, which were multiplied with the band formulae (e.g. 28.072 in model 1 of Tab. 5). The intercepts are the positive or negative number in each model (e.g. +0.5785 in model 1 of Tab. 5). Please see other slopes and intercepts for model no. 2 to model no. 26 in Tab. 5. The range of r^2 for all empirical models was from 0.01 to 0.91. The correlation coefficients <0.50 were considered weak due to which we regarded only the models with $r^2 > 0.50$ (model no.1 to model no.14 in Tab. 5) as significant [36]. Among these significant models, r^2 was higher (i.e. 0.73–0.91) for the models with red band (e.g. model no. 1 to model no. 8 in Tab. 5) whereas it was lower (i.e. 0.54–0.72) in the models without red band (e.g. model no. 10 to model no. 14 in Tab. 5). The best model was the use of the spectral band R (i.e. $r^2 = 0.91$, see model no. 1 in Tab. 5). The scatter plot and deviation plot of this model are shown in Fig. 2a and b. The figure shows that 10 data records matched 100% of the modeled values, whereas four data records had a deviation of 1 from the modeled values (Fig. 2b). The result of this validation indicates the usefulness of this model for obtaining CWQI from the reflectance of the red band.

Most of the previous studies showed the development of remote sensing based models for individual water quality variables, e.g. [8–18]. A limited number of studies showed the application of remote sensing for the development of indices [37, 38]. Composite pollution index was developed using band 1 (0.402–0.422 μm), band 2 (0.433–0.453 μm), band 3 (0.480–0.500 μm), and band 4 (0.500–0.520 μm) to obtain the five classes of water quality. The co-efficient of determination for the composite pollution index was 0.93 [37]. In another study, remote sensing based water quality index was developed on the basis of blue and green bands. The r^2 was 0.82 for this water quality index [38]. In our study, we found that the models with: (i) blue and green bands (e.g. model 13 in Tab. 5), (ii) green band (e.g. model 10 in Tab. 5), (iii) blue band (e.g. model 19 in Tab. 5) showed r^2 of 0.57, 0.71, and 0.30, respectively. It was also noticed that the models having blue and green band with: (i) red band (e.g. model 7 in Tab. 5), and (ii) red and NIR bands (e.g. model 6 in Tab. 5) showed higher values for r^2 (i.e. 0.75 and 0.76, respectively).

3.2 Empirical models for obtaining turbidity classes

We created 26 empirical models for turbidity as given in Tab. 6, which could be used to obtain the spatial distribution of turbidity using the planetary reflectance of bands for a period of interest. The slopes and

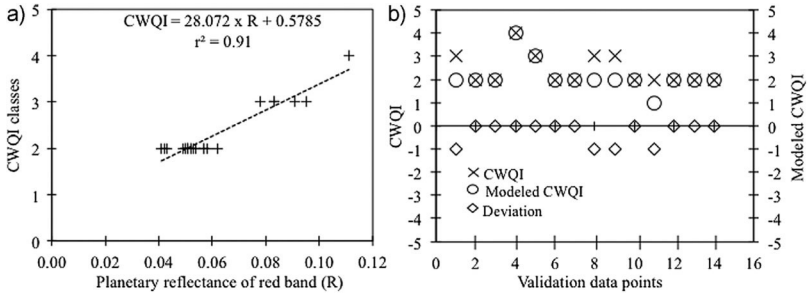

Figure 2. (a) Development, and (b) evaluation of most suitable model for obtaining CWQI classes using the surface reflectance of red band for the Bow River.

Table 6. Models developed for mapping spatial distribution of turbidity for the Bow River using the first four spectral bands (i.e. blue, green, red, and NIR) of Landsat-5 TM satellite data

Model no.	Model	r^2	Model no.	Model	r^2
1	1005 R − 44.608	0.82	14	530.92 (B + NIR) − 55.95	0.47
2	533.51 (G + R) − 59.624	0.77	15	−30.533 (B/R) + 66.455	0.32
3	567.88 (R + NIR) − 42.301	0.73	16	−30.041 [(B/R) + R] + 67.509	0.29
4	385.17 (G + R + NIR) − 54.932	0.73	17	−30.076 [(B/R) + G] + 68.198	0.29
5	368.42 (B + G + R) − 70.666	0.69	18	−28.74 [(B/R) + B] + 66.277	0.29
6	295.94 (B + G + R + NIR) − 66.185	0.69	19	630.78 B − 42.417	0.27
7	187.38 (R/G) − 120.43	0.66	20	32.406 (R/B) − 4.4814	0.13
8	531.38 (B + R) − 65.694	0.66	21	−7.1225 [(B/NIR) + G] + 34.532	0.07
9	1059.2 G − 70.18	0.66	22	−7.1171 [(B/NIR) + B] + 34.604	0.07
10	595.17 (G + NIR) − 57.657	0.65	23	33.057 [(NIR/B) + NIR] + 0.1987	0.08
11	387.37 (B + G + NIR) − 68.127	0.59	24	51.506 (NIR/G) − 9.6089	0.07
12	516.81 (B + G) − 73.428	0.52	25	28.779 (NIR/B) + 3.641	0.05
13	1062.7 NIR − 28.796	0.49	26	6.8317 (G/B) + 11.017	0.01

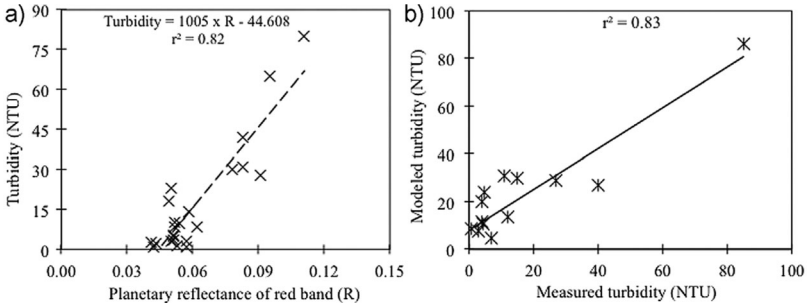

Figure 3. (a) Development, and (b) evaluation of most suitable model for obtaining turbidity using the surface reflectance of red band for the Bow River.

intercepts for the empirical models (i.e. model no. 1 to model no. 26) of turbidity are given in Tab. 6. The range of r^2 for the models was from 0.01 to 0.82. Similar to CWQI empirical models, we considered only the models with $r^2 > 0.50$ (model no. 1 to model no. 12 in Tab. 6) as significant and the all models with $r^2 < 0.50$ were weak [36]. Similar to CWQI models, r^2 was higher (i.e. 0.66–0.82 for the considerable models with red band (e.g. model no. 1 to model no. 8 in Tab. 6), whereas it was lower (i.e. 0.52–0.66) for the models without red band (e.g. model no. 9 to model no. 12 in Tab. 6). Among all the models, the best model was the use of the spectral band R (i.e. $r^2 = 0.82$, see model no. 1 in Tab. 6) and its development is also described in Fig. 3a. We evaluated the turbidity model (i.e. model no. 1 given in Tab. 6) using the validation data of the ground measured turbidity data as shown in Fig. 3b. The validation indicated a strong correlation of modeled turbidity with the measured turbidity by giving $r^2 = 0.83$ which is even higher as compared to r^2 obtained for turbidity model. These results suggest the usefulness of this model (i.e. model no.1 given in Tab. 6) for mapping turbidity from Landsat-5 TM satellite data for the Bow River. The red band also correlated well with in situ turbidity in other studies. r^2 values in these studies were 0.78, 0.76, and 0.57, respectively [7, 12, 13].

3.3 Application of models for spatial and temporal analysis

We applied the best (i) CWQI model (i.e. model no. 1 in Tab. 5), and (ii) turbidity determination model (i.e. model no. 1 in Tab. 6) over all 31 scenes of Landsat-5 TM during the period 2006–2010 for generating the spatial distribution of CWQI and turbidity classes for the Bow River. The examples of classes for CWQI and turbidity are shown over a portion of the Bow River in Figs. 4 and 5, respectively. The percentages for five CWQI classes and six turbidity classes observed in each year during the period 2006–2010 are given in Tabs. 7 and 8, respectively. The deteriorated quality of water could be estimated from the percentages accumulated in each year for the CWQI classes of 4 and 5. Those were: (i) 2.62% in 2006, (ii) 32.75% in 2007, (iii) 4.77% in 2008, (iv) 1.46% in 2009, (v) 6.94% in 2010, and (vi) 9.71% during 2006–2010 in average. On this basis, we might rank the years in order from the best to the worst water quality, such as: 2009, 2006, 2008, 2010, and 2007. Turbidity also showed similar ranks for the respective years on the basis of percentages for the worst turbidity class (i.e. >50 NTU). The variation in the water quality for different years could be related to surface runoff from different amount of precipitations due to climatic factors like snowmelt and rainfall [6].

The impact of natural sub-regions was reflected on the river water quality classification in Tab. 9. We found that the prominent CWQI

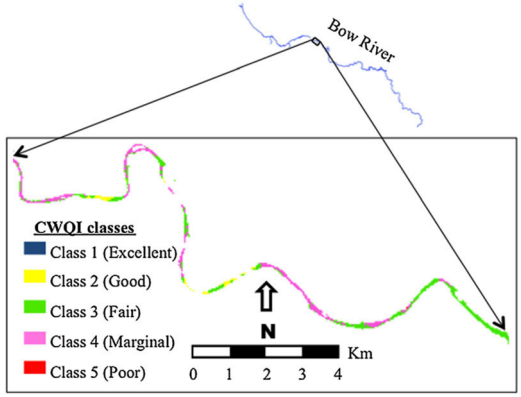

Figure 4. An example of CWQI classes for ~14 km long portion of the Bow River obtained by application of the most suitable empirical model (i.e. model no. 1 in Tab. 4) on Landsat-5 TM satellite image dated 21 June 2007.

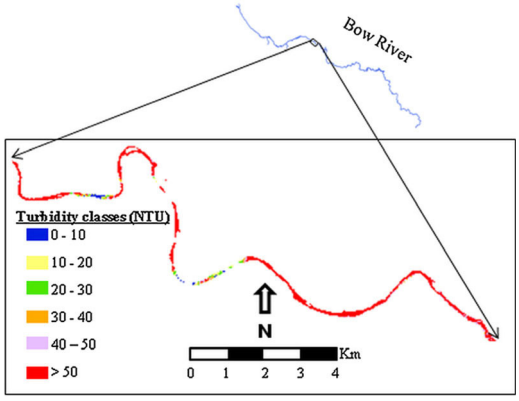

Figure 5. An example of turbidity classes for ~14 km long portion of the Bow River obtained by application of the most suitable empirical model (i.e. model no. 1 in Tab. 5) on Landsat-5 TM satellite image dated 21 June 2007.

Table 7. Percentages of CWQI classes for each year during 2006–2010

CWQI class	Percentage (%) of CWQI classes					
	2006	2007	2008	2009	2010	2006–2010
1	0.10	0.45	0.06	0.05	1.51	0.44
2	72.66	40.83	39.42	73.78	62.69	57.88
3	24.62	25.97	55.74	24.71	28.85	31.98
4	2.29	32.01	4.16	1.06	6.87	9.28
5	0.33	0.74	0.62	0.40	0.08	0.43

Table 8. Percentages of turbidity classes for each year during 2006–2010

Turbidity class (NTU)	Percentage (%) of turbidity classes				
	2006	2007	2008	2009	2010
0–10	24.40	11.18	10.91	19.37	12.86
10–20	36.22	19.64	18.72	41.90	28.17
20–30	24.08	16.60	16.24	18.90	27.05
30–40	6.88	9.29	21.30	10.66	9.15
40–50	3.92	4.27	22.57	6.06	8.99
>50	4.49	39.02	10.26	3.10	13.78

Table 9. Dominant CWQI classes for Bow River in natural sub-regions for selected scenes of Landsat-5 TM

Landsat-5 TM scene data	Dominant CWQI classes for				
	Dry mixed grass	Mixed grass	Foothills fescue	Foothills parkland	Montane
24 April 2006	2	3	2	–	–
21 June 2007	4	4	4	4	3
23 July 2007	–	3	2	3	3
29 April 2008	3	4	3	–	–
18 July 2008	2	3	2	–	–
21 July 2009	2	2	2	–	–
25 Oct. 2009	3	2	2	–	–
15 July 2010	–	3	2	2	2
19 April 2010	3	3	2	–	–

classes were (i) class 3 or class 4 for mixed grass, and (ii) class 3 for dry mixed grass. The deteriorated water quality for the Bow River in both of these natural regions could be related to irrigation-based farming [39]. During the summer months, we observed class 3 and class 4 for Bow River in foothills parkland, foothills fescue and montane. This deterioration in the Bow river water quality in these three sub-regions could be due to till cropping (i.e. short-season crops) [39].

4 Concluding remarks

In this research, we developed empirical models for Canadian Water Quality Index (CWQI) and turbidity using the planetary reflectance data from the first four bands (i.e. blue, green, red, and NIR) of Landsat-5 TM for the Bow River of Alberta. The data utilized for the development and evaluation of these models included 31 scenes of Landsat-5 TM multispectral images, CWQI classes based on the monthly measured ground data for 17 water quality variables, and in situ monthly measured turbidity data for a period of five years (i.e. 2006–2010). For CWQI, we created 26 models of which 14 were significant based on the co-efficient of determination (r^2) ranging from 0.54 to 0.91. Likewise for turbidity, we developed 26 models of which 12 were significant based on r^2 ranging from 0.52 to 0.82. For both CWQI and turbidity, the models with highest r^2 (i.e. 0.91 and 0.82, respectively) were evaluated and applied on all 31 scenes to obtain classes for CWQI and turbidity for the Bow River during 2006–2010. The red band was found to be the most important as it dominated eight CWQI models and eight turbidity models with higher range of r^2 values with its solitary contribution in the best models. The turbidity classes showed similar patterns of water quality in each year of interest as exhibited by the CWQI classes. The river water quality was deteriorated due to agricultural activities and climatic factors. The limitation of using 30 m resolution satellite data was the contamination of river water pixels caused by influence of nearby land covers/uses. To overcome this in our research, we made use of NDVI to recognize such pixels and eliminate them from the images.

Acknowledgments

We acknowledge Natural Sciences and Engineering Research Council of Canada (NSERC) for providing "Postgraduate Scholarship at Doctoral level (PGS-D3)" to Tahir Ali Akbar. We also acknowledge United States Geological Survey (USGS) for providing the satellite data and Alberta Environment for providing water quality data.

The authors have declared no conflict of interest.

References

[1] International Decade for Action 'Water for Life' 2005–2015, *Why a 'Water for Life' Decade?*, United Nations Department of Economic and Social Affairs (UNDESA), Zaragoza, Spain **2005**.

[2] P. H. Gleick, *Water in Crisis: A Guide to the World's Freshwater Resources*, Oxford University Press, New York **1993**, p. 13.

[3] Water Quality, *Fresh Water Quality Monitoring & Surveillance*, Environment Canada, Gatineau, QC **2012**.

[4] S. A. Telang, Effects of Reservoir-Dam, Urban, Industrial, and Sewage Treatment Run-Off on the Presence of Oxygen and Organic Compounds in the Bow River, *Water Air Soil Pollut.* **1990**, *50*, 77–90.

[5] Canadian Council of Ministers of the Environment, *Canadian Water Quality Index 1.0, Technical Report and User's Manual*, Canadian

Environmental Quality Guidelines Water Quality Index Technical Subcommittee, Gatineau, QC, Canada **2001**.

[6] T. A. Akbar, Q. K. Hassan, G. Achari, Clusterization of Surface Water Quality and Its Relation to Climate and Land Use/Cover, *J. Environ. Prot.* **2013**, *4*, 333–343.

[7] M. J. Moreno-Madrinan, M. Z. Al-Hamdan, D. L. Rickman, F. E. Muller-Karger, Using the Surface Reflectance MODIS Terra Product to Estimate Turbidity in Tampa Bay, Florida, *Remote Sens.* **2010**, *2*, 2713–2728.

[8] V. Sládeček, Satellite Imagery in Distinguishing the Water Quality, *Acta Hydrochim. Hydrobiol.* **2006**, *17*, 609–617.

[9] L. G. Olmanson, P. L. Brezonik, M. E. Bauer, Airborne Hyperspectral Remote Sensing to Assess Spatial Distribution of Water Quality Characteristics in Large Rivers: The Mississippi River and Its Tributaries in Minnesota, *Remote Sens. Environ.* **2013**, *130*, 254–265.

[10] S. Stisen, K. H. Jensen, I. Sandholt, D. I. F. Grimes, A Remote Sensing Driven Distributed Hydrological Model of the Senegal River Basin, *J. Hydrol.* **2008**, *354*, 131–148.

[11] E. Alparslan, C. Aydöner, V. Tufekci, H. Tüfekci, Water Quality Assessment at Ömerli Dam Using Remote Sensing Techniques, *Environ. Monit. Assess.* **2007**, *135*, 391–398.

[12] J. Bustamante, F. Pacios, R. DÍaz-Delgado, D. Aragonés, Predictive Models of Turbidity and Water Depth in the Doñana Marshes Using Landsat TM and ETM+ Images, *J. Environ. Manage.* **2009**, *90*, 2219–2225.

[13] B. Nas, S. Ekercin, H. Karabörk, A. Berktay, D. J. Mulla, An Application of Landsat-5 TM Image Data for Water Quality Mapping in Lake Beysehir, Turkey, *Water Air Soil Pollut.* **2010**, *212*, 183–197.

[14] F. L. Hellweger, P. Schlosser, U. Lall, J. K. Weissel, Use of Satellite Imagery for Water Quality Studies in New York Harbor, *Estuarine Coastal Shelf Sci.* **2004**, *61*, 437–448.

[15] M. Wu, W. Zhang, X. Wang, D. Luo, Application of MODIS Satellite Data in Monitoring Water Quality Parameters of Chaohu Lake in China, *Environ. Monit. Assess.* **2009**, *148*, 255–264.

[16] D. W. Bolgrien, N. G. Granin, L. Levin, Surface-Temperature Dynamics of Lake Baikal Observed from AVHRR Images, *Photogramm. Eng. Remote Sens.* **1995**, *61*, 211–216.

[17] A. G. Dekker, R. J. Vos, S. W. M. Peters, Analytical Algorithms for Lake Water TSM Estimation for Retrospective Analyzes of TM and SPOT Sensor Data, *Int. J. Remote Sens.* **2002**, *23*, 15–35.

[18] Y. Oyama, B. Matsushita, T. Fukushimaa, K. Matsushige, A. Imai, Application of Spectral Decomposition Algorithm for Mapping Water Quality in a Turbid Lake (Lake Kasumigaura, Japan) from Landsat TM Data, *ISPRS J. Photogramm. Remote Sens.* **2009**, *64*, 73–85.

[19] F. Wang, L. Han, T. Kung, R. B. van Arsdale, Applications of Landsat-5 TM Imagery in Assessing and Mapping Water Quality in Reelfoot Lake, Tennessee, *Int. J. Remote Sens.* **2006**, *27*, 5269–5283.

[20] Statistics Canada, *Population and Dwelling Counts, for Canada, Provinces and Territories, and Census Subdivisions (Municipalities) 2011*, Censuses, Statistics Canada, Alberta, Canada **2012**.

[21] M. Seneka, *Trends in Historical Annual Flows for Major Rivers in Alberta*, Environmental Monitoring and Evaluation Branch, Environmental Assurance, Alberta Environment, Government of Alberta, Alberta, Canada **2004**.

[22] K. M. Jeffries, E. R. Nelson, L. J. Jackson, R. H. Habibi, Basin-Wide Impacts of Compounds with Estrogen-Like Activity on Longnose Dace (*Rhinichthys cataractae*) in Two Prairie Rivers of Alberta, Canada, *Environ. Toxicol. Chem.* **2008**, *27*, 2042–2052.

[23] M. Bennett, M. Murray, *Bow River Basin, State of the Watershed Summary 2010*, Bow River Basin Council, Calgary Water Centre, Calgary, Alberta, Canada **2010**, p. 5.

[24] United States Geological Survey (USGS), *USGS Global Visualization Viewer*, Earth Resources Observation and Science Center (EROS), United States Geological Survey, Reston, VA **2012**.

[25] National Aeronautics and Space Administration (NASA), *Landsat Processing Details*, United States Geological Survey, Reston, VA **2012**.

[26] Alberta Environment and Sustainable Resource Development, *Alberta River Water Quality Index: Objectives, Water Data, Environment and Water*, Government of Alberta, Ottawa **2011**.

[27] Alberta Environment, *Surface Water Quality Guidelines for Use in Alberta*, Science and Standards Branch, Environmental Assurance Division, Edmonton, Alberta **1999**.

[28] Health Canada, *Guidelines for Canadian Drinking Water Quality*, Federal-Provincial-Territorial Committee on Drinking Water of the Federal-Provincial-Territorial Committee on Health and the Environment, Ottawa, Ontario, Canada **2010**.

[29] Ontario Drinking Water Standards, *Technical Support Document for Ontario Drinking Water Standards, Objectives and Guidelines*, Ministry of the Environment, Drinking Water Ontario, Government of Ontario, Canada **2006**.

[30] National Aeronautics and Space Administration (NASA), *Landsat 7 Science Data Users Handbook*, National Aeronautics and Space Administration, Washington, DC **2011**.

[31] G. Chander, B. Markham, Revised Landsat-5 TM, Radiometric Calibration Procedures and Postcalibration, Dynamic Ranges, *IEEE Trans. Geosci. Remote Sens.* **2003**, *41*, 2674–2677.

[32] C. J. Tucker, Red and Photographic Infrared Linear Combinations for Monitoring Vegetation, *Remote Sens. Environ.* **1979**, *8*, 127–150.

[33] J. Weier, D. Herring, *Measuring Vegetation (NDVI & EVI)*, NASA Earth Observatory, Washington, DC **1999**.

[34] CliffsNotes, *Simple Linear Regression*, Houghton Mifflin Harcourt Publishing Company, Boston, Massachusetts, USA **2013**.

[35] R. M. Cox, R. D. Forsythe, G. E. Vaughan, L. L. Olmsted, Assessing Water Quality in Catawba River Reservoirs Using Landsat Thematic Mapper Satellite Data, *Lakes Reservoirs Res. Manage.* **1998**, *14*, 405.

[36] F. Roberts, D. Roberts, *Correlation Coefficient*, Mathbits, New York **2013**.

[37] C. Chen, Z. Pan, P. Shi, H. Zhan, Application of Satellite Data for Integrated Assessment of Water Quality in the Pearl River Estuary, China, *Geoscience and Remote Sensing Symp., IGARSS Proc., IEEE International*, Vol. 4, Seoul **2005**, pp. 2550–2553.

[38] A. Vignolo, A. Pochettino, D. Cicerone, Water Quality Assessment Using Remote Sensing Techniques: Medrano Creek, Argentina, *J. Environ. Manage.* **2006**, *81*, 429–433.

[39] D. J. Downing, W. W. Pettapiece, *Natural Regions and Subregions of Alberta*, Natural Regions Committee, Government of Alberta, Alberta, Canada **2006**.

